RESEARCH ARTICLE

Key Points:
- Long-term fCO_2 in coastal South Atlantic Bight is increasing at a rate greater than open ocean
- The fCO_2 increase is likely a combination of increases from terrestrial sources, with little to no influence from temperature
- The related pH decrease on this coastal margin is likely greater than that of the open ocean

Supporting Information:
- Supporting Information S1
- Figure S1
- Figure S2
- Figure S3

Correspondence to:
W.-J. Cai,
wcai@udel.edu

Multidecadal *f*CO₂ Increase Along the United States Southeast Coastal Margin

Janet J. Reimer[1], Hongjie Wang[2] (ID), Rodrigo Vargas[3] (ID), and Wei-Jun Cai[1] (ID)

[1]School of Marine Science and Policy, University of Delaware, Newark, DE, USA, [2]Department of Physical and Environmental Sciences, Texas A&M, Corpus Christi, TX, USA, [3]Department of Plant and Soil Sciences, University of Delaware, Newark, DE, USA

Abstract Coastal margins could be hotspots for acidification due to terrestrial-influenced CO_2 sources. Currently there are no long-term (>20 years) records from biologically important coastal environments that could demonstrate sea surface CO_2 fugacity (fCO_2) and pH trends. Here, multidecadal fCO_2 trends are calculated from underway and moored time series observations along the United States southeast coastal margin, also referred to as the South Atlantic Bight (SAB). fCO_2 trends across the SAB, derived from ~26 years of cruises and ~9.5 years from a moored time series, range from 3.0 to 4.5 μatm yr^{-1}, and are greater than the open ocean increases. The pH decline related to the fCO_2 increases could be as much as -0.004 yr^{-1}; a rate greater than that expected from atmospheric-influenced pH alone. We provide evidence that fCO_2 increases and pH decreases on an ocean margin can be faster than those predicted for the open ocean from atmospheric influence alone. We conclude that a substantial fCO_2 increase across the marginal SAB is due to both increasing temperature on the middle and outer shelves, but to lateral land-ocean interactions in the coastal zone and on inner shelf.

1. Introduction

Increased CO_2 fugacity (fCO_2) in the global surface ocean has been linked to increasing atmospheric CO_2 since the onset of the Industrial Revolution, and is also the primary cause of long-term decreases in surface ocean pH and carbonate mineral saturation state (Sabine et al., 2004; Takahashi et al., 2009, 2014). Long-term fCO_2 trends, and attribution, in the open surface ocean are reasonably well estimated due to the relative stability of the open ocean (as compared with coastal sites) (Fay & McKinley, 2013; McKinley et al., 2016). It is more challenging, however, to determine long-term changes in fCO_2 on coastal margins due to large spatiotemporal variations from various potential sources and sinks of fCO_2 (Bauer et al., 2013; Jiang et al., 2008; Xue et al., 2016). Understanding long-term trends in fCO_2, the primary driver of ocean acidification (OA) (Sabine et al., 2004), is necessary for predicting the response of ocean margin pH and OA (Wootton et al., 2008), and to assess the vulnerability of many marine organisms living in coastal environments (Ekstrom et al., 2015; Kroeker et al., 2013; Waldbusser & Salisbury, 2014). Currently, there are no long-term (>20 years) estimates from coastal margins, which are biologically and socioeconomically important, that demonstrate trends in sea surface fCO_2 and pH trends.

Several relatively short-time series (<10 years) have been used to demonstrate coastal fCO_2 trends, which have resulted in a range of estimates over diverse ecosystems around the world. North Sea CO_2 partial pressure (pCO_2) in the (summer 2001 versus summer 2005) increased at a rate 5–6 times faster than the atmosphere (10 to 12 μatm yr^{-1}, Thomas et al., 2007), although another report found a slower increase (4 μatm yr^{-1} over the summers of 2005 and 2008) (Salt et al., 2013). In the northern South China Sea, pCO_2 is increasing only slightly faster than that of the atmosphere (Tseng et al., 2007). Conversely, 8 years of sea surface pCO_2 observations in the NW Atlantic Ocean north of Puerto Rico indicate that there is no increase in winter sea surface pCO_2, leading to an increase in the regional sink for the atmospheric CO_2 (Park & Wanninkhof, 2012). Along the Japanese and European margins the CO_2 increase is similar to that of the atmosphere (Wang et al., 2016a) and the open North Atlantic increase of ~2 μatm yr^{-1} (Bates, 2007). Both fCO_2 and pCO_2 are reported in the literature; fortunately, this is not a serious issue as the difference between fCO_2 and pCO_2 generally less than measurement uncertainty (< 2 μatm). The range of estimates for marginal sea CO_2 concentration changes are likely due to the different factors contributing to variability, which

is driven by the type of environment, though many CO_2 rates, such as the aforementioned values, on coastal margins are greater than atmospheric and open ocean estimates. Therefore, region-specific studies are crucial for determining how different environments respond to changes in the carbonate system due to fCO_2 and for reducing uncertainty in global carbon budgets.

Here we derive an estimate of multidecadal fCO_2 change along the United States southeast coastal margin, also known as the South Atlantic Bight (SAB), using in situ observations spanning >25 years. The SAB coastal margin is characterized by moderate river inputs and extensive biologically and social-economically important salt marshes. Since moored fCO_2 time series are still rather new and cruises are sporadic, we compare both types of observations across the SAB. Using empirical linear methods, an examination of deseasonalization, and a generalized additive mixed model (GAMM) (Wang et al., 2016a), we show that simple linear and GAMM techniques agree well across SAB regions. After calculating fCO_2 trends across the SAB, we apply the fCO_2 change to pH to determine a potential associated pH trend.

2. Methods

2.1. Site Description

The SAB extends from Cape Hatteras in the north to Cape Canaveral in the south, and out to the continental shelf break. The SAB is a relatively wide, shallow shelf with 10 small to medium-sized rivers that empty into the surrounding coastal wetlands before entering the SAB. The largest river, with the most extensive watershed region that empties into the SAB is the Altamaha River, with the mouth located just northwest of the Gray's Reef (GR) moored CO_2 time series. The mean position of the core of the Gulf Stream runs along the 200 m isobath, extending seaward and landward on both sides of the isobath (Castelao, 2011), directly affecting both the middle and outer shelf regions. Mesoscale encroachment onto the inner shelf (shoreward of the 20 m isobath) rarely occurs (Castelao & He, 2013). A southward flowing, cooler, fresher current flows along the coast, which is more prominent when freshwater discharge from the various rivers increases (Menzel, 1993).

We propose different delineations of the SAB shelf regions as compared to previous studies, such that fCO_2 gradients may diminish within the new definition of regions. Previously, the shelf regions were defined as up to 20 m (i.e., inner shelf), 20–40 (i.e., middle shelf), and 40–60 m (i.e., outer shelf) (Jiang et al., 2008; Menzel, 1993). Due to relatively high fCO_2 in the estuaries (values may exceed 1,200 μatm; Cai & Wang, 1998) and river plumes, with resulting intense spatial gradients (Jiang et al., 2008), we divide the traditional inner shelf into two sections: from the seaward side of the barrier islands to up to 15 m (i.e., coastal region) and then 15–30 m (i.e., inner shelf). The middle shelf is then extended to 30–60 m and the outer region from 60 to over 200 m (Figure 1). We divided underway fCO_2 observations into these regions based on the depth (isobath). Since not all data sets over the 26 years of cruises provide depth, we sectioned the cruise tracts into their regions using Latitude and Longitude along the isobaths. Therefore, this framework harmonizes the diverse efforts to make isobaths comparable across campaigns.

2.2. Moored Autonomous Time Series

fCO_2 is from the National Oceanographic and Atmospheric Administration's (NOAA) Moored Autonomous pCO_2 (MAPCO$_2$) time series on the Gray's Reef (GR) mooring located on the inner shelf (NDBC-41008 at 31.400°N, −80.868°W). The GR mooring time series has been recording fCO_2 since July 2006 at a frequency of 3 h, averaged to one day for analyses herein. Data quality control was initially carried out by NOAA upon receiving the data. We then applied a secondary quality assessment to determine data points potentially influenced by biofouling and other contamination, random outliers, and gap-filling (using linear interpolation) for gaps no longer than 2 days (using the daily mean time series). Extensive validation of this time series is presented in Reimer et al. (2017). We present observations through 15 October 2015, which provide just less than a decade of observations. Furthermore, we present over 20 years of daily (averaged from hourly frequency) SST observations from the GR mooring and the Edisto mooring, on the middle shelf (NDBC-41004 at 32.501°N, −79.099°W), to explore possible influence of thermal contributions to fCO_2 trends. Gulf Stream intrusions are frequent on the middle shelf (Castelao, 2011, 2014; Lee et al., 1991), where the Edisto mooring is located in approximately 40 m of water just southeast of Charleston, SC.
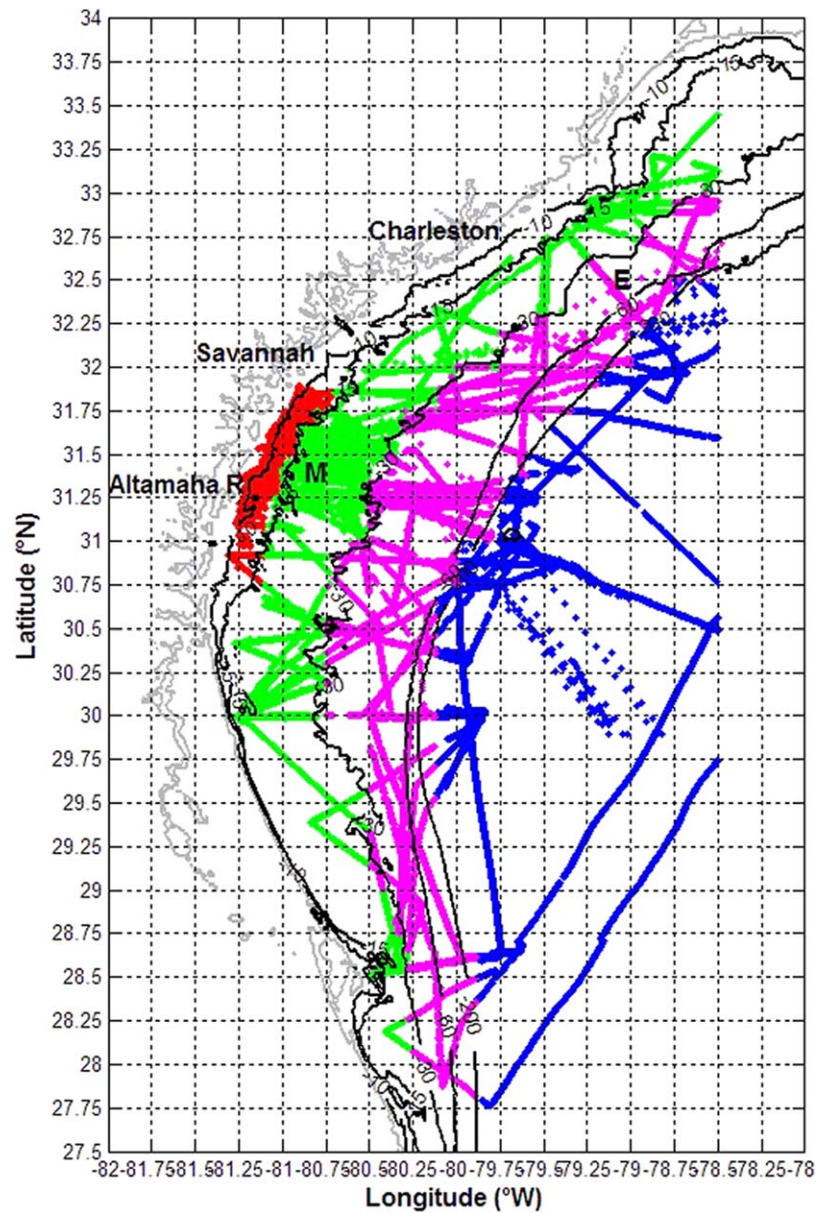
Figure 1. Delineation of the SAB shelf regions analyzed in this study, the locations of the Gray's Reef mooring (M on the map) on the inner shelf, and the Edisto mooring (E on the map) on the middle shelf. The black lines are the 10, 15 30, 60, and 200 m isobaths (from west to east).

2.3. Underway Observations

Supporting information Table S1 gives a summary of the 26 years of cruises used in this study. All underway data from the earliest vessel of opportunity (VOO) cruises in the 1990s provide fCO_2, sea surface temperature (SST), latitude, and longitude; however, sea surface salinity (SSS) is from the 2004 version of the World Ocean Database (WOD). The other cruises report all the data necessary to calculate fCO_2 from the raw data provided (partially dry mole fraction of CO_2, SST, SSS, and atmospheric pressure) (Sutton et al., 2014). All observations are averaged to daily values within each spatial region for linear trend analysis, however, the GAMM (see below) does not use daily values.

2.4. Trend Determination, Deseasonalization, and Seasonal Cycles

It can be difficult to discern trends even in multidecadal time series, particularly in coastal settings, with high variability due to large excursions (Fay & McKinley, 2013). We address this challenge by reducing large

excursion in the time series via deseasonalization and by comparing statistical methods. To analyze the trends (i.e., slope of the linear least squares best-fit line) in daily frequency time series, we use linear least squares applied to deseasonalized fCO_2 observations over time, with 95% confidence intervals (CI's). Traditionally, deseasonalization is a method in which the mean seasonal harmonic signals are removed from the time series, leaving only the anomalous excursions from the mean. The fCO_2 time series (moored and underway) is deseasonalized using a long-term mean "reference year" (supporting information Figure S1), therefore deseasonalized values are observed fCO_2 minus a reference value. The reference values are determined over a theoretical reference year, which is a mean for each day of the year from all the fCO_2 observations over the time series (for approximately 9 years); such that the reference value for 1 January is a mean of all the 1 January values. Initially, outliers, defined as plus or minus three times the standard deviation of the mean for each day, in raw data were not included in the calculation of the reference year daily values. Undetected outliers in the final and deseasonalized time series, which are identified through a robust linear model algorithm with weighted values, are excluded from linear slope (trend) calculations. In theory, the GAMM (see below) compensates for extreme outliers, therefore removal of outliers is not necessary as part of the data treatment.

We derive a deseasonalization method using a long-term mean reference year, rather than a single year (Takahashi et al., 2009) and verify the ability of long-term mean to remove seasonal signals by comparing our method to a known rate of CO_2 increase. After applying the aforementioned method, we compared our reference year deseasonalization method to other methods and with additional data sets. First, we tested the time series mean method on observation of dry mole fraction CO_2 (xCO_2) values in the air from the Tudor Hill, Bermuda Institute of Ocean Sciences (BIOS) site (GlobalView station) and GR mooring air values. The BIOS observations demonstrate long-term trends in the air. Deseasonalization comparisons are discussed in detail below. Then, to further assess how much of the seasonal cycle in the moored xCO_2 (raw data prior to fCO_2 calculation) time series is removed, we apply a mean harmonic method (Fay & McKinley, 2013), which also provides a comparison of seasonal cycles for the GAMM method (see below). The BIOS observations are only available in the dry mole fraction (denoted as xCO_2); however, the mean difference between CO_2 at saturation (partial pressure or fugacity) and the dry mole fraction is -0.7 ± 0.4 in the air at the GR mooring over the time series from 2006 through 2015.

Daily underway means are calculated from all the values from a given shelf region for each day and then deseasonalized with the reference year. Given underway observations are not equally distributed over time and space, we are unable to derive a climatological reference year specific to each SAB region from moored observations. We recognize that there are latitudinal and longitudinal differences across the SAB, however, we aim to show that this deseasonalization method provides reasonable results given the general spatio-temporal limitations if using a reference year to deseasonalize. Regional trends with 95% CI's are then determined from the deseasonalized time series using a linear least squares approach. Linear models assume that the observations are homoscedastic, therefore, deseasonalization prior to trend calculation can reduce heteroscedasticity in the data set. Given that linear methods may not fully meet the homoscedastic assumption, we apply the GAMM method to compare to the results of the linear models for the time series of underway observations.

2.5. Generalized Additive Mixed Model for Underway Observations

Briefly, generalized additive mixed modeling is a statistical method that uses observed SST, SSS, fCO_2, location, and time (Wang et al., 2016a, 2017). The GAMM method predicts fCO_2 primarily based on three terms derived from observations: seasonal cycle (time and inherent seasonal biogeochemical signals), environmental covariates (in this instance SST and SSS), and the long-term sea surface fCO_2 change. Sampling date (seasonal signal) in the GAMM is a linear effect, and its coefficient represents the fCO_2 trend. Essentially, fCO_2 changes that cannot be explained by seasonal cycle, SST, and SSS variations represent the fCO_2 temporal trend (fCO_2 trend × year).

After the underway observations were sectioned into their respective SAB regions, we also applied the GAMM to deseasonalize and determine linear trends and 95% CI's for these spatial data sets. Here, we use all observations, not daily mean values. The GAMM, which is a spatiotemporal model, is only applied to underway observations in this case to compare to linear results. Furthermore, since cruises are highly temporally sporadic with respect to the moored time series, the seasonal cycle can be more challenging to

identify. Briefly, the GAMM calculates the fCO_2 trend by combining the penalized spline fitting of the seasonal cycle, second-degree polynomials fitting of the SST, SSS, and their interaction, and linear fitting of the long-term rate (equation (1)) (Wang et al., 2016a, 2017). The fCO_2 trend is calculated as:

$$fCO_2 = \text{spline(Julian day)} + f(\text{SST, SSS}) + \text{slope} \times \text{time} \qquad (1)$$

where the spline fit is the a function of Julian day, f(SST, SSS) describes the nonlinear function (influence) of SST and SSS (predictor variables) to decycled fCO_2, and the slope is the daily fCO_2 trend. The GAMM method is not applicable to SST and SSS trends as we do not have appropriate predictor variables, other than time, for their best-fit equations. Given that moored time series for SST, predictor of thermal fCO_2 variability, is available on a daily frequency in two of the three regions, we use the higher-frequency observations to determine linear trends rather than the GAMM for this variable. We note that if other biogeochemical predictor variables (e.g., carbonate system variables, respiration, and/or biomass) were available for all cruises, then these other predictors could be incorporated into the GAMM method. Even though the spatiotemporal availability of directly measured biogeochemical variables are limited, the other variables already included in GAMM analysis (time, SST, and SSS) all contains some level of biological signal as they reflect river inputs, seasonal biological change, and seasonal water mass advective patterns.

2.6. pH Change Due to fCO_2 Change

To determine the rate of change in pH due to the total change in fCO_2 (fCO_2 due to atmospheric adsorption, biological activity, thermal influence, and advection) over the time series, we calculate pH in CO2SYS (Dickson & Millero, 1987; Lee et al., 2010; Lewis & Wallace, 1998) and determine the slope over a yearly pH time series. The steps of the calculation are as follows:

1. Total alkalinity (TA) for the mean sea surface salinity (SSS) for each region of the SAB was determined from the TA-SSS relationship:

$$TA = 44.66 \text{ SSS} + 573.63 \qquad (2)$$

This relationship was determined by Xue et al. (2016) from samples across all four of the SAB shelf regions. We assume that the TA is constant over time across the shelf due to historical perspective that the ocean is relatively well buffered. This may not be the case in the coastal or inner regions of the SAB; however, for the purposes of this initial estimate and first attempt at assessing pH in the SAB, we maintain this assumption.

2. The second variable used in CO2SYS is fCO_2. Using a starting value of 350 μatm (the same value used in the calculation to determine the potential thermal influence) in year 1991, we increase the fCO_2 every year by the mean annual growth rate for each region (Table 1 of the main text). We demonstrate the potential change in pH using both the linear least-squares trends and the GAMM trends to give a range based on the method used.

Table 1
Long-Term Mean Deseasonalization and GAMM Trend Results

Region/ mooring	fCO_2 (μatm), pH, or SST (°C yr^{-1})	95% CI (μatm or °C yr^{-1})	Best-fit $y = mx + b$; p-value	GAMM fCO_2 or pH (μatm yr^{-1})	95% CI (μatm yr^{-1})
Outer fCO_2	3.0	3.2	$fCO_2 = 0.0082 \times \text{time} - 6{,}012$; $p < 0.001$	3.3	0.3
Outer pH	−0.003	5.3×10^{-5}		−0.003	6.3×10^{-5}
Middle fCO_2	3.2	2.3	$fCO_2 = 0.0089 \times \text{time} - 6{,}575$; $p < 0.001$	4.1	0.4
Middle pH	−0.003	6.0×10^{-5}		−0.004	9.4×10^{-5}
Edisto (SST)	0.07	0.03	$\text{SST} = 0.0002 \times \text{time} - 125$; $p < 0.001$		
Inner fCO_2	3.7	2.2	$fCO_2 = 0.0201 \times \text{time} - 14{,}408$; $p < 0.001$	4.5	0.6
Inner pH	−0.003	7.9×10^{-5}		−0.004	1.2×10^{-5}
GR (fCO_2)	3.5	0.9	$fCO_2 = 0.0096 \times \text{time} - 25$; $p < 0.001$		
GR pH	−0.003*	4.5×10^{-5}			
GR (SST)	−0.05	0.04	$\text{SST} = -0.0001 \times \text{time} - 118$; $p < 0.001$		
Coastal fCO_2	3.2	5.2	$fCO_2 = 0.0087 \times \text{time} - 6{,}389$; $p < 0.05$	3.4	1.3
Coastal pH	−0.003	6.1×10^{-5}		−0.003	6.9×10^{-5}

Note. Trends (second and fifth columns) and 95% CI's are calculated by multiplying the slope and 95% CI range (daily time step) by 356 to obtain a yearly value. The p-values for the best-fit lines indicate the level at which the relationship is significant, and the 95% CI's provide a level of confidence for the trend. If the 95% CI crosses zero, then the trend may not be significant, as in the coastal region even though the p-value of the relationship is significant. GAMM p-values are <0.001.

3. The input values for CO2SYS are the mean SSS, SST, calculated TA (for each region's mean SSS), a pressure value of zero, and the increasing $f\mathrm{CO}_2$. Given the determined SST change on the middle (and outer) shelf, we run the calculation a second time including the 0.07°C SST change (Table 1 of the main text and supporting information Figure S2). The results including the SST change were not statistically different than those without.
4. The calculated yearly pH is regressed (linear least-squares) over time (1991–2016) to determine the linear change in pH (Table 1). We do not include an analysis of GR mooring pH because it is assumed that it is well represented within the 95% CI range of the inner shelf $f\mathrm{CO}_2$ trend.

3. Results

Previous methods that have used a mean of the data set or one specific reference value to deseasonalize (Takahashi et al., 2009) do not remove as much of the seasonal signal as using a long-term mean (Figure 2). The Tudor Hill air trend is 1.8 ± 0.4 µatm yr^{-1} and the GR deseasonalized $x\mathrm{CO}_2$ and nondeseasonalized air trends are 2.2 ± 0.1 and 2.3 ± 0.2 µatm yr^{-1}, respectively. Though not statistically different, the confidence interval for the deseasonalized trend is lower. Therefore, the long-term mean method to deseasonalize CO_2 observations could provide an improved method over using a time series mean as in Takahashi et al. (2009) when multiple years are available. Even after deseasonalization with the long-term mean, GR observations
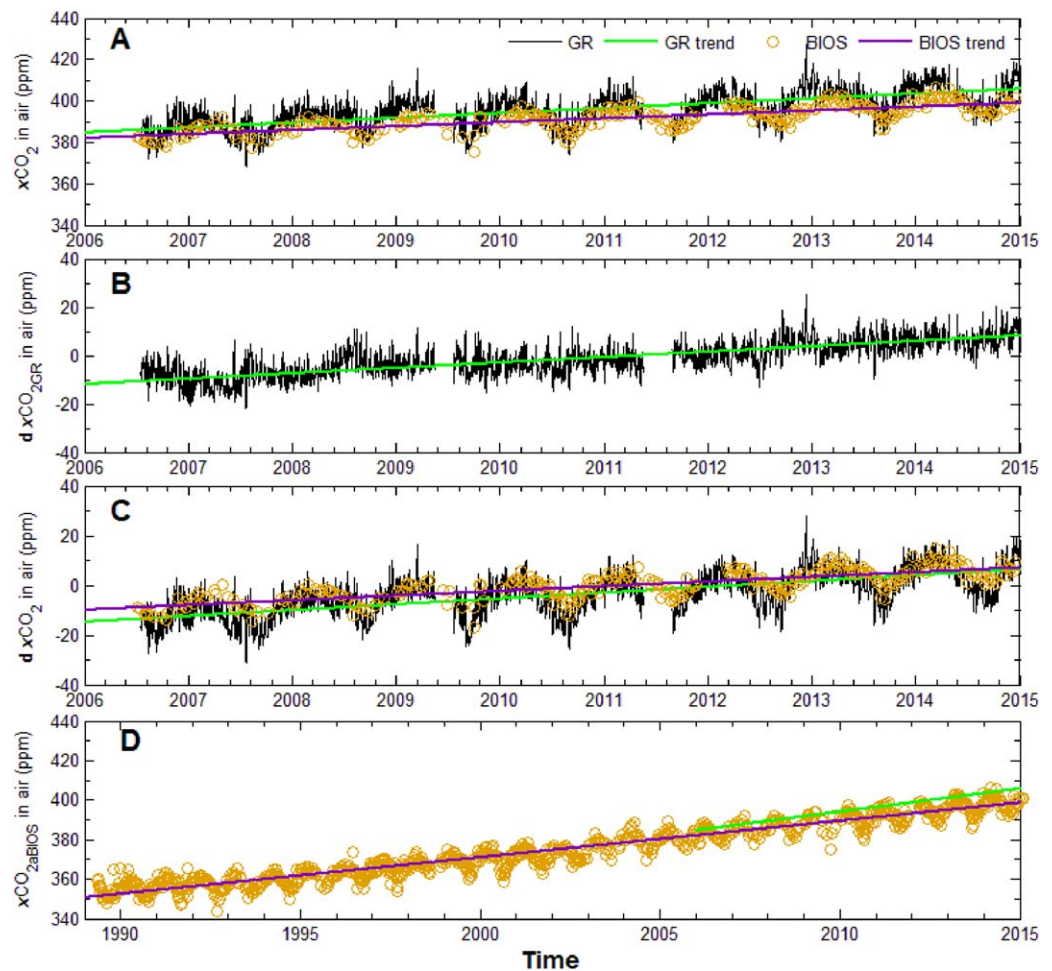

Figure 2. (a) The virtually parallel linear trends (within the 95% CI) for air $x\mathrm{CO}_2$ at the GR mooring and BIOS $x\mathrm{CO}_{2air}$ over the period of the moored series. (b) The linear trend for deseasonalized GR air $x\mathrm{CO}_2$ (d$x\mathrm{CO}_{2GR}$) using the long-term year method; slopes in Figures 2a and 2b are not statistically different. (c) Deseasonalized GR and BIOS air $x\mathrm{CO}_2$ using respective time series means after Takahashi et al. (2009). (d) The linear trend for 25 years of BIOS $x\mathrm{CO}_{2air}$ and the trend for d$x\mathrm{CO}_{2GR}$.

reveal a relatively small fCO_2 maxima in the late summer/early fall (supporting information Figure S3) that was not removed. This residual seasonality is similar to the second maxima identified in underway measurements via the GAMM (supporting information Figure S3).

Daily mean SAB fCO_2 (Figure 3a), as well as deseasonalized values (Figure 3b), is greatest in the coastal region and decreases across the shelf. fCO_2 trends from both the least squares and GAMM within the four regions of the SAB exhibit results that are not statistically different, with estimates ranging from 3.0 to 4.5 $\mu atm\ yr^{-1}$ (Table 1). 95% CI's calculated for the GAMM are narrower than those for least squares (Table 1). The fCO_2 trend from GR ($3.5 \pm 0.9\ \mu atm\ yr^{-1}$; Table 1) is also similar to trends for SAB regions using both statistical approaches (Figures 3b and 3c). The GAMM results in slightly greater fCO_2 trends than linear deseasonalization; however, the linear method 95% CI's, which represent variability in the trends, overlap with GAMM results. Considering the determined fCO_2 increases across the SAB and for both the GAMM and linear methods, pH decreases from 0.003 to 0.004 units yr^{-1} (Table 1).

SST from GR on the inner shelf is not increasing; rather there is statistically significant decline ($-0.05 \pm 0.04°C\ yr^{-1}$; Table 1). SST from the moored Edisto time series on the middle shelf, however, is increasing at a rate of $0.07 \pm 0.03°C\ yr^{-1}$ (Table 1), or $1.82 \pm 0.78°C$ (1994 through 2016). The SST range on the inner and middle shelves typically reach similar yearly maxima, though over the time series winters on the inner shelf are cooler, while middle shelf winters are warmer than they were in the beginning of the time series (supporting information Figure S2).
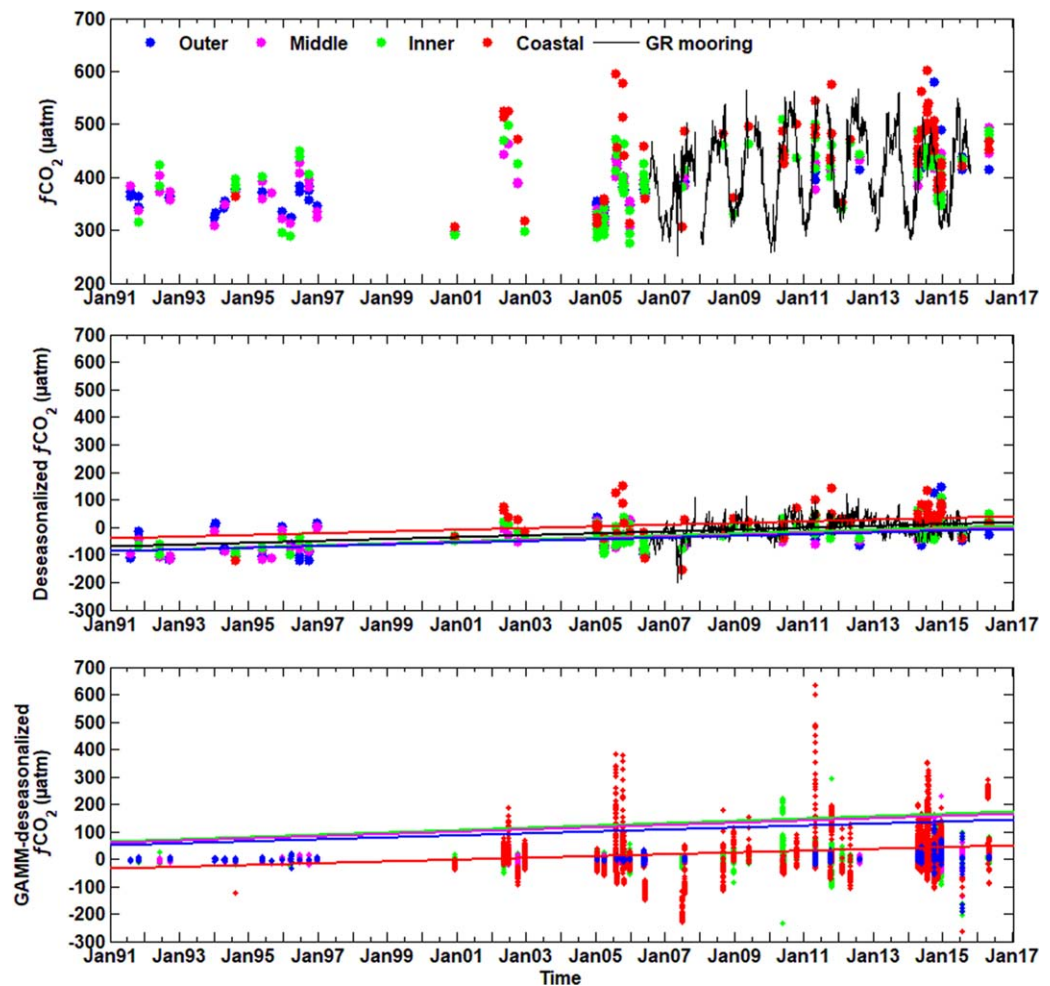

Figure 3. (a) Time series of daily mean cruise (dots) and GR fCO_2 observations. (b) Time series of deseasonalized cruise and mooring fCO_2 with regional trend lines using the long-term mean method and (c) the GAMM.

4. Discussion

4.1. Deseasonalization Methods

The test case for air $x\mathrm{CO_2}$ shows that using a long-term mean reference year gives similar trend results to the mean global increase since the Industrial Revolution. Furthermore, results are consistent with the global increase in the open surface ocean of approximately 2 µatm yr^{-1}, which is known to closely follow the atmospheric trend (Bates et al., 2012; Sabine et al., 2004). The BIOS (and overall atmospheric) trend is variable over its lifetime, with a growth rate of ~1.5 ppm yr^{-1} in the 1990s to 2.0 ppm yr^{-1} in the 2000s (https://www.esrl.noaa.gov/gmd/ccgg/trends/gr.html). Therefore, these comparisons provide evidence that our relatively short-time series (GR mooring <10 years) provide consistent and robust trend estimates.

We find good agreement between the two approaches for determining $f\mathrm{CO_2}$ trends across the SAB. The GAMM identified a slightly different seasonal signal than the long-term mean method, and the trends were slightly higher with narrower confidence intervals. The large confidence intervals from the linear method overlap with GAMM trends; therefore, the methods provide trend results that are not statistically different (Table 1). Ultimately, the GAMM takes into account some of the nonlinearity associated with environmental variability (SST and SSS), and could provide a better assessment of trends, as well as lower uncertainty, in highly variable data sets. We note that GAMM deseasonalization brings the early 1990s observations close to zero anomalies, whereas the reference year creates a large negative anomaly (Figure 3). While the reference year method is affected by the years used to create it, we find that it can still provide reasonable results for the middle and outer shelves in this study and is also a suitable method to use if more sophisticated trend determination methods are not available to the user. Since a greater portion of the seasonal signal was removed by the GAMM to deseasonalize the observations prior to trend analysis, the observed lower uncertainty (95% CI) is expected. A considerable drawback of the GAMM method is that it will not function without predictor variables (SST and SSS, among others), though given the ever increasing wealth of data in public repositories, this not likely to be a major issue for data mining underway observations. The reference year method, however, is likely a better option for the growing field of moored data sets where it removes much of the seasonal cycle (Figures 2 and 3). For the purposes of our results, we present the discussion based on both methods.

4.2. Multidecadal Results: Trends and Uncertainty

The increasing SAB $f\mathrm{CO_2}$ trends, determined using both long-term mean deseasonalization and GAMM methods, are greater than the global atmospheric increase, as well as the mean global surface ocean increase, of approximately 2 µatm yr^{-1}. We assume that 2 µatm yr^{-1} of the SAB regional, and GR, $f\mathrm{CO_2}$ time series increases are due to the increase in atmospheric $\mathrm{CO_2}$. Then, we interpret that the remaining portion of the trend is due to one or more of the following: $f\mathrm{CO_2}$ lateral/horizontal transport, biological addition, or long-term thermal influences (Fay & McKinley, 2013; Takahashi et al., 2009), which is discussed in the next section. Given that there are likely different factors that influence trends in each region, we do not lump them together to determine the cause of the increases on each region of the shelf. It should be noted, however, that while the coastal region and the inner shelf exhibit larger seasonal variability than the middle and outer shelves, the linear method still derives similar trends across the SAB. The trends across the SAB and at GR likely indicate that the long-term mean deseasonalization and linear trend calculation is reliable and that a common factor among the various shelf regions is driving the $f\mathrm{CO_2}$ increase on this coastal margin.

The 95% CI's for both methods represent intrinsic variability across space and time and highlight the dynamic nature of marginal $f\mathrm{CO_2}$. The 95% CI's calculated via the long-term mean method are greater than those for the GAMM, likely because of the residual seasonal signal that was not removed via long-term mean deseasonalization (supporting information Figure S3), especially in the case of the coastal region where $f\mathrm{CO_2}$ ranged from ~300 to >600 µatm. The occasional large excursions away from the climatological mean (Figure 3b) are likely important on shorter than multidecadal time scales; however, the results of the present work suggest that increased tends from the multidecadal analyses tend to move toward equilibrium with the atmosphere, as was previously determined for open ocean regions (McKinley et al., 2011). For example, in a previous short-term analysis of only GR $\mathrm{CO_2}$ from July of 2006 through October of 2014, the increase was up to ~5 µatm yr^{-1} (Reimer et al., 2017). Extending the length of time covered by the moored time series, by using the underway observations, even though they are relatively sporadic,

results in a weaker fCO_2 increase. Thus, the noisy time series is muted over longer time scales as in the open ocean (McKinley et al., 2016).

4.3. Trend Attribution

We postulate that nonthermal processes are influencing the overall fCO_2 increase on the inner shelf or GR. High fCO_2 waters from the coastal marshes are likely advected seaward across the shelf due to river outflow and tidal exchanges (Cai et al., 2003; Jiang et al., 2013; Xue et al., 2016). Water mass residence and travel times across the inner shelf are ~1–3 months (Menzel, 1993; Moore, 2007; Xue et al., 2016), and depend on river stream flow volume from the local rivers (Sheldon & Alber, 2015). Furthermore, respiration (biological addition) of the organic materials advected seaward is also a likely fCO_2 source in the coastal region and inner shelf (Cai & Wang, 1998; Jiang et al., 2013; Sheldon & Alber, 2015; Sheldon et al., 2010). Therefore, laterally advected high fCO_2 and organic matter-rich waters are a likely source for increased fCO_2 in the coastal region and the inner shelf.

Given the available observations, we are unable to decompose the trends into all of their components, which can limit our ability to assign specific values to all the mechanistic processes involved. We can, however, use the information that we have to eliminate thermal processes as a major influence on the inner shelf. Anomalies identified via deseasonalization give us insights into the episodic drivers, such as pulses of high fCO_2 waters from the coastal region (e.g., influx of organic matter, nutrients, and DIC) (Sheldon & Alber, 2013, 2015). Episodic pulses greatly influence the shorter-term trend, however, these pulses are damped over long-time periods (Fay & McKinley, 2013), unless they become more frequent or a new normal under climate change scenarios (IPCC, 2014). The mechanistic importance of eustatic sea level rise is another process that we are unable to quantify at this time. Sea level disturbances on sediments and losses of coastal wetlands, such as those due to sea level increases over the last few decades, result in CO_2 and organic material liberation to the overlaying water (Duarte et al., 2013; Macreadie et al., 2013). Future global sea level rise could influence the amount of fCO_2 transported away from the coastal zone as more carbon-rich coastal wetlands are lost, thus influencing fCO_2 on coastal margins.

On the middle shelf SST is increasing by 0.07°C yr^{-1}, thus the resulting SST effect, assuming an fCO_2 of 350 µatm (mean of all observations from 1991) at the beginning of the time series, is: $0.07 \times 350 \times 4.3\% = 1.1$ µatm yr^{-1} (Takahashi et al., 1993). The thermally driven trend could contribute 1.1 µatm, with the remaining 2–3 µatm yr^{-1} increase due to air-sea gas exchange and other processes, including contributions from river and marsh fCO_2 and organic matter respiration (Jiang et al., 2013; Xue et al., 2016). Similarly, the open North Atlantic fCO_2 trend is also dominated by nonthermal components, identified as the air-sea exchange with minimal chemical changes due to respiration and transport (McKinley et al., 2011). Therefore, terrestrial processes likely still dominate the SAB middle shelf trend, with the atmospheric component contributing up to ~2 µatm yr^{-1} (from the atmospheric and open ocean increases). The warmer winters on the middle shelf (supporting information Figure S2) could influence fCO_2 in this region. Further research into potentially warming waters offshore in the SAB would be necessary to answer this question.

Finally, our most densely sampled portion of the outer shelf is also close to, or within the core of the Gulf Stream; therefore, we assume that it has common mechanistic trend drivers as the middle shelf and that Gulf Stream characteristics, such as SST and fCO_2, likely drive the positive trend. A portion of Gulf Stream fCO_2, as dissolved inorganic carbon (DIC), could be transported from the Gulf of Mexico (via the Loop Current), which receives increasing DIC from the Mississippi River (Ren et al., 2015). DIC could also be from respired organic matter during transit from the Gulf of Mexico or across the SAB shelf (Jiang et al., 2010; Wang et al., 2013). At this time, we do not have information on Gulf Stream specific characteristics or its location; however, it is impossible to ignore that regional transport processes could supply CO_2 to the SAB.

Despite all trends being statistically similar, it is likely that the different mechanistic processes that influence the four shelf regions vary in terms of their relative importance. In the coastal region and on the inner shelf thermal processes do not contribute to the fCO_2 trend, whereas thermal processes contribute up to a third of fCO_2 increase on the middle and outer shelves. The differing relevance of the drivers highlights the disparity in coastal versus open ocean acidification. Nonetheless, within the entire SAB all trends are more rapid than in the open ocean, indicating a common source that we attribute to increased river and marsh export of high fCO_2 water with subsequent respiration of exported organic matter. Furthermore, DIC transport out of marshes increases due to tidally mediated transport (Wang et al., 2016b), which could be a

corollary to sea level rise. As sea level increases, more DIC is likely to be transported out of coastal marshes to shelf regions (Bauer et al., 2013), therefore, transport processes could become even more important drivers of carbonate chemistry on continental margins in the future. Isolating the nonthermal contributions to fCO_2 trends on continental margins is an important step in determining vulnerability to acidification, and should be the focus of future studies in the SAB and continental margins.

4.4. pH Trends Due to fCO_2 Increases

We provide evidence for large pH decreases (Table 1) in the SAB that range from -0.003 units yr^{-1} (for fCO_2 trends in the coastal ocean calculated with the long-term mean deseasonalization method) to -0.004 units yr^{-1} (on the inner and middle shelves using the GAMM method). Increasing SST trends on the middle and outer shelves did not change the results of the pH trend calculation (see supporting information). Our rate is more rapid than the open ocean rate, which is approximately -0.002 pH units yr^{-1}, and is thought to occur in the majority of the open ocean (IPCC, 2014). Our calculated pH change agrees qualitatively with other studies that have determined that there is a decrease in pH with increasing CO_2 (Takahashi et al., 2014; Sabine et al., 2004; Sutton et al., 2016; Wootton et al., 2008), although our decrease is faster than the atmospheric-based prediction. The pH decrease in the SAB takes into account only fCO_2 changes, assuming that total alkalinity (TA) is not changing over time (see supporting information). If this assumption is not justified and TA does not remain constant over time, or decreases, then shelf water buffering capacity will decreases as fCO_2 increases (Cai et al., 2010; Wang et al., 2013). Therefore, the ratio of DIC to TA increases, which results in decreased pH. This change would make the coastal waters in SAB more vulnerable to future acidification stress.

5. Concluding Remarks

Here we introduce an alternative method to deseasonalize fCO_2 prior to linear trend assessments, which achieves results that are similar to the more complex GAMM. One or both of the methods could be employed in other regions. Both methods conclude that fCO_2 across the SAB, a coastal margin influenced by abundant freshwater discharge and a strong, warm ocean current (Gulf Stream), is increasing faster than the atmospheric trend. Consequently, pH on this coastal margin is decreasing more rapidly than in the open ocean. This study highlights the importance of trend determination in different marginal seas, as environmental contributions can be distinct within a single shelf region, as well as in different parts of the world. Apart from the assumed ~2 $\mu atm\ yr^{-1}$ atmospheric CO_2 contribution to SAB increasing trends, we find that the thermal influence on the middle shelf is likely responsible for only one third of the region's increase. On the inner shelf, however, thermal influence is not likely contributing to the increase. Rather, the source of increasing fCO_2 on the inner shelf and coastal region could be from the atmosphere and contributions via transport processes from the coastal rivers, estuaries, and marshes. Marsh DIC contributions may become more important in marginal environments as sea level continues to rise. We suggest two primary paths for future research in the SAB and beyond: (1) quantification of the remaining nonthermal influences, apart from air-sea exchange; (2) the seasonal to long-term effects of increased fCO_2 and other carbonate system variables, and their sources of variability, on the state of acidification on coastal margins influenced by freshwater.

References

Bates, N. R. (2007). Interannual variability of the oceanic CO 2 sink in the subtropical gyre of the North Atlantic Ocean over the last 2 decades. *Journal of Geophysical Research*, 112, C09013. https://doi.org/10.1029/2006JC003759

Bates, N. R., Best, M. H. P., Neely, K., Garley, R., Dickson, A. G., & Johnson, R. J. (2012). Detecting anthropogenic carbon dioxide uptake and ocean acidification in the North Atlantic Ocean. *Biogeosciences*, 9(7), 2509–2522. https://doi.org/10.5194/bg-9-2509-2012

Bauer, J. E., Cai, W., Raymond, P. A., Bianchi, T. S., Hopkinson, C. S., & Regnier, P. A. G. (2013). The changing carbon cycle of the coastal ocean. *Nature*, 504, 61–70. https://doi.org/10.1038/nature12857

Cai, W.-J., Hu, X., Huang, W.-J., Jiang, L.-Q., Wang, Y., Peng, T.-H., & Zhang, X. (2010). Alkalinity distribution in the western North Atlantic Ocean margins. *Journal of Geophysical Research*, 115, C08014. https://doi.org/10.1029/2009JC005482

Cai, W.-J., & Wang, Y. (1998). The chemistry, fluxes, and sources of carbon dioxide in the estuarine waters of the Satilla and Altamaha Rivers, Georgia. *Limnology and Oceanography*, 43(4), 657–668. https://doi.org/10.4319/lo.1998.43.4.0657

Cai, W.-J., Wang, Z. A., & Wang, Y. (2003). The role of marsh-dominated heterotrophic continental margins in transport of CO 2 between the atmosphere, the land-sea interface and the ocean. *Geophysical Research Letters*, 30(16), 1849. https://doi.org/10.1029/2003GL017633

Castelao, R. (2011). Intrusions of Gulf Stream waters onto the South Atlantic Bight shelf. *Journal of Geophysical Research*, *116*, C10011. https://doi.org/10.1029/2011JC007178

Castelao, R. M. (2014). Mesoscale eddies in the South Atlantic Bight and the Gulf Stream Recirculation region: Vertical structure. *Journal of Geophysical Research: Oceans*, *119*, 2048–2065. https://doi.org/10.1002/2014JC009796

Castelao, R. M., & He, R. (2013). Mesoscale eddies in the South Atlantic Bight. *Journal of Geophysical Research: Oceans*, *118*, 5720–5731. https://doi.org/10.1002/jgrc.20415

Dickson, A. G., & Millero, F. J. (1987). A comparison of the equilibrium constants for the dissociation of carbonic acid in seawater media. *Deep Sea Research Part A*, *34*(10), 1733–1743. https://doi.org/10.1016/0198-0149(87)90021-5

Duarte, C. M., Losada, I. J., Hendriks, I. E., Mazarrasa, I., & Marba, N. (2013). The role of coastal plant communities for climate change mitigation and adaptation. *Nature Climate Change*, *3*(11), 961–968. Retrieved from https://doi.org/10.1038/nclimate1970; http://www.nature.com/nclimate/journal/v3/n11/abs/nclimate1970.html#supplementary-information

Ekstrom, J. A., Suatoni, L., Cooley, S. R., Pendleton, L. H., Waldbusser, G. G., Cinner, J. E., . . . Portela, R. (2015). Vulnerability and adaptation of US shellfisheries to ocean acidification. *Nature Climate Change*, *5*(3), 207–214. https://doi.org/10.1038/nclimate2508

Fay, A. R., & McKinley, G. A. (2013). Global trends in surface ocean p CO 2 from in situ data. *Global Biogeochemical Cycles*, *27*, 541–557. https://doi.org/10.1002/gbc.20051

IPCC (2014). IPCC, 2014: Climate change 2014: Impacts, adaptation, and vulnerability. Part A: Global and sectoral aspects. In C. B. Field et al. (Eds.), *Contribution of working group II to the fifth assessment report of the intergovernmental panel on climate change* (1132 p.). Cambridge, UK: Cambridge University Press.

Jiang, L.-Q., Cai, W.-J., Wang, Y., & Bauer, J. E. (2013). Influence of terrestrial inputs on continental shelf carbon dioxide. *Biogeosciences*, *10*, (1–1. 22, https://doi.org/10.5194/bg-10-1-2013

Jiang, L.-Q., Cai, W.-J., Wang, Y., Diaz, J., Yager, P. L., & Hu, X. (2010). Pelagic community respiration on the continental shelf off Georgia, USA. *Biogeochemistry*, *98*(1–3), 101–113. https://doi.org/10.1007/s10533-009-9379-8

Jiang, L.-Q., Cai, W.-J., Wanninkhof, R., Wang, Y., & Lüger, H. (2008). Air-sea CO 2 fluxes on the U.S. South Atlantic Bight: Spatial and seasonal variability. *Journal of Geophysical Research*, *113*, C07019. https://doi.org/10.1029/2007JC004366

Kroeker, K. J., Kordas, R. L., Crim, R., Hendriks, I. E., Ramajo, L., Singh, G. S., . . . Gattuso, J. P. (2013). Impacts of ocean acidification on marine organisms: Quantifying sensitivities and interaction with warming. *Global Change Biology*, *19*(6), 1884–1896. https://doi.org/10.1111/gcb.12179

Lee, K., Kim, T. W., Byrne, R. H., Millero, F. J., Feely, R. A., & Liu, Y. M. (2010). The universal ratio of boron to chlorinity for the North Pacific and North Atlantic oceans. *Geochimica et Cosmochimica Acta*, *74*(6), 1801–1811. https://doi.org/10.1016/j.gca.2009.12.027

Lee, T., Yoder, J., & Atkinson, L. (1991). Gulf Stream frontal eddy influence on productivity of the southeast US continental shelf. *Journal of Geophysical Research*, *96*, 191–205.

Lewis, E., & Wallace, D. (1998). *Program developed for CO2 system calculations* (ORNL/CDIAC 105). Oak Ridge, TN: Carbon Dioxide Information Analysis Center, Oak Ridge National Laboratory, U.S. Department of Energy.

Macreadie, P. I., Hughes, A. R., & Kimbro, D. L. (2013). Loss of "Blue Carbon" from coastal salt marshes following habitat disturbance. *PLoS One*, *8*(7), e69244. https://doi.org/10.1371/journal.pone.0069244

McKinley, G. A., Fay, A. R., Takahashi, T., & Metzl, N. (2011). Convergence of atmospheric and North Atlantic carbon dioxide trends on multidecadal timescales. *Nature Geoscience*, *4*(9), 606–610. https://doi.org/10.1038/ngeo1193

McKinley, G. A., Pilcher, D. J., Fay, A. R., Lindsay, K., Long, M. C., & Lovenduski, N. S. (2016). Timescales for detection of trends in the ocean carbon sink. *Nature*, *530*(7591), 469–472. https://doi.org/10.1038/nature16958

Menzel, D. (1993). *Ocean processes: US southeast continental shelf* (DOE/OSTI-1, 121 p.). Oak Ridge, TN: U.S. Department of Energy, Office of Technical Information.

Moore, W. S. (2007). Seasonal distribution and flux of radium isotopes on the southeastern U.S. continental shelf. *Journal of Geophysical Research*, *112*, C10013. https://doi.org/10.1029/2007JC004199

Park, G.-H., & Wanninkhof, R. (2012). A large increase of the CO2 sink in the western tropical North Atlantic from 2002 to 2009. *Journal of Geophysical Research*, *117*, C08029. https://doi.org/10.1029/2011JC007803

Reimer, J. J., Cai, W.-J., Xue, L., Vargas, R., Noakes, S., Hu, X., . . . Wanninkhof, R. (2017). Time series pCO2 at a coastal mooring: Internal consistency, seasonal cycles, and interannual variability. *Continental Shelf Research*, *145*, 95–108. https://doi.org/10.1016/j.csr.2017.06.022

Ren, W., Tian, H., Tao, B., Yang, J., Pan, S., Cai, W. J., . . . Hopkinson, C. S. (2015). Large increase in dissolved inorganic carbon flux from the Mississippi River to Gulf of Mexico due to climatic and anthropogenic changes over the 21st century. *Journal of Geophysical Research: Biogeosciences*, *120*, 724–736. https://doi.org/10.1002/2014JG002761

Sabine, C. L., Feeley, R. A., Gruber, N., Key, R. M., Lee, K., Bullister, J. L., . . .Rios, A. F. (2004). The oceanic sink for anthropogenic CO2. *Science*, *305*(5682), 367–371. https://doi.org/10.1126/science.1097403

Salt, L. A., Thomas, H., Prowe, A. E. F., Borges, A. V., Bozec, Y., & De Baar, H. J. W. (2013). Variability of North Sea pH and CO2 in response to North Atlantic Oscillation forcing. *Journal of Geophysical Research: Biogeosciences*, *118*, 1584–1592. https://doi.org/10.1002/2013JG002306

Sheldon, J. E., & Alber, M. (2013). *Effects of climate signals on river discharge to Ossabaw, St. Andrew, and Cumberland sounds*. Athens, GA: Georgia Coastal Research Council.

Sheldon, J. E., & Alber, M. (2015). Comparing transport times through salinity zones in the Ogeechee and Altamaha River estuaries using squeezebox. In K. J. Hatcher (Ed.), *Proceedings of the 2005 Georgia water resources conference*. Athens, GA: Institute of Ecology, University of Georgia.

Sheldon, J. E., Griffith, P. C., Peters, F., Sheldon, W. M., Blanton, J. O., Amft, J., & Pomeroy, L. R. (2010). Southeastern U.S.A. continental shelf respiratory rates revisited. *Biogeochemistry*, *107*, 501–506. https://doi.org/10.1007/s10533-010-9552-0

Sutton, A. J., Sabine, C. L., Feely, R. A., Cai, W.-J., Cronin, M. F., McPhaden M. J., . . . Weller, R. A. (2016). Using present-day observations to detect when anthropogenic change forces surface ocean carbonate chemistry outside pre-industrial bounds. *Biogeosciences*, *13*, 5065–5083. https://doi.org/10.5194/bg-2016-104

Sutton, A. J., Sabine, C. L., Maenner-Jones, S., Lawrence-Slavas, N., Meinig, C., Feely, R. A., . . . Kozyr, A. (2014). A high-frequency atmospheric and seawater pCO2 data set from 14 open ocean sites using a moored autonomous system. *Earth System Science Data*, *6*(2), 353–366. https://doi.org/10.5194/essdd-7-385-2014

Takahashi, T., Olafsson, J., Goddard, J., Chipman, D., & Sutherland, S. (1993). Seasonal variation of CO2 and nutrients in the high-latitude surface oceans: A comparative study. *Global Biogeochemical Cycles*, *7*, 843–878.

Takahashi, T., Sutherland, S. C., Chipman, D. W., Goddard, J. G., Cheng, H., Newberger, T., . . . Munro, D. R. (2014). Climatological distributions of pH, pCO2, total CO2, alkalinity, and CaCO3 saturation in the global surface ocean, and temporal changes at selected locations. *Marine Chemistry*, *164*, 95–125. https://doi.org/10.1016/j.marchem.2014.06.004

Takahashi, T., Sutherland, S. C., Wanninkhof, R., Sweeney, C., Feely, R. A., Chipman, D. W., . . . de Baar, H. J. W. (2009). Climatological mean and decadal change in surface ocean pCO2, and net sea–air CO2 flux over the global oceans. *Deep Sea Research Part II: Topical Studies in Oceanography*, *56*(8–10), 554–577. https://doi.org/10.1016/j.dsr2.2008.12.009

Thomas, H., Friederike Prowe, A. E., van Heuven, S., Bozec, Y., de Baar, H. J. W., Schiettecatte, L.-S., . . . Doney, S. C. (2007). Rapid decline of the CO2 buffering capacity in the North Sea and implications for the North Atlantic Ocean. *Global Biogeochemical Cycles*, *21*, GB4001. https://doi.org/10.1029/2006GB002825

Tseng, C.-M., Wong, G. T. F., Chou, W.-C., Lee, B.-S., Sheu, D.-D., & Liu, K.-K. (2007). Temporal variations in the carbonate system in the upper layer at the SEATS station. *Deep Sea Research Part II: Topical Studies in Oceanography*, *54*(14–15), 1448–1468. https://doi.org/10.1016/j.dsr2.2007.05.003

Waldbusser, G. G., & Salisbury, J. E. (2014). Ocean acidification in the coastal zone from an organism's perspective: Multiple system parameters, frequency domains, and habitats. *Annual Review of Marine Science*, *6*, 221–247. https://doi.org/10.1146/annurev-marine-121211-172238

Wang, H., Hu, X., Cai, W.-J., & Sterba-Boatwright, B. (2017). Decadal fCO$_2$ trends in global ocean margins and adjacent boundary current-influenced areas. *Geophysical Research Letters*, *44*, 8962–8970. https://doi.org/10.1002/2017GL074724

Wang, H., Hu, X., & Sterba-Boatwright, B. (2016a). A new statistical approach for interpreting oceanic fCO$_2$ data. *Marine Chemistry*, *183*, 41–49. https://doi.org/10.1016/j.marchem.2016.05.007

Wang, Z. A., Kroeger, K. D., Ganju, N. K., Gonneea, M. E., & Chu, S. N. (2016b). Intertidal salt marshes as an important source of inorganic carbon to the coastal ocean. *Limnology and Oceanography*, *61*(5), 1916–1931. https://doi.org/10.1002/lno.10347

Wang, Z. A., Wanninkhof, R., Cai, W.-J., Byrne, R. H., Hu, X., Peng, T.-H., & Huang, W.-J. (2013). The marine inorganic carbon system along the Gulf of Mexico and Atlantic coasts of the United States: Insights from a transregional coastal carbon study. *Limnology and Oceanography*, *58*(1), 325–342. https://doi.org/10.4319/lo.2013.58.1.0325

Wootton, J. T., Pfister, C. A., & Forester, J. D. (2008). Dynamic patterns and ecological impacts of declining ocean pH in a high-resolution multi-year dataset. *Proceedings of National Academy of Sciences of the United States of America*, *105*(48), 18848–18853. https://doi.org/10.1073/pnas.0810079105

Xue, L., Cai, W. J., Hu, X., Sabine, C., Jones, S., Sutton, A. J., . . . Reimer, J. J. (2016). Sea surface carbon dioxide at the Georgia time series site (2006–2007): Air-sea flux and controlling processes. *Progress in Oceanography*, *140*, 14–26. https://doi.org/10.1016/j.pocean.2015.09.008

Multi-decadal *f*CO$_2$ increase along the United States southeast coastal margin

Janet J. Reimer[1], Hongjie Wang[2], Rodrigo Vargas[3], and Wei-Jun Cai[1]*

[1]School of Marine Science and Policy, University of Delaware, Newark DE, 19716

[2]Texas A&M, Department of Physical and Environmental Sciences, Corpus Christi TX, 78412

[3] Department of Plant and Soil Sciences, University of Delaware, Newark, DE 19716

Contents of this file

Introduction

The Supporting Information contains the details of the specific cruises used in this work (Table S1), as well as two graphics. The first graphic (Figure S1) one examines the seasonal cycles of *f*CO$_2$. Determination of seasonal cycles is an intermediate step for determining the long-term trend. The second graphic (Figure S2) is the long-term trends of sea surface temperature (SST).
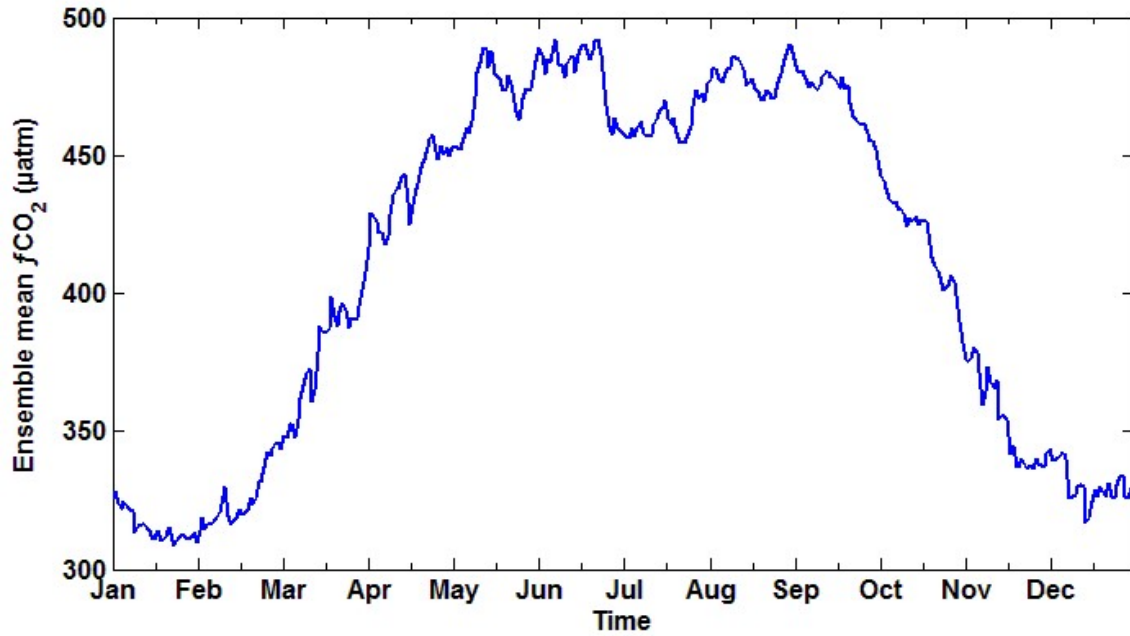
Figure S1. The ensemble mean reference year used to deseasonalize fCO_2 across the SAB shelf. The smoothed seasonal cycle identified by the GAMM is similar to the ensemble mean in that there are two distinct maxima over the warm months.
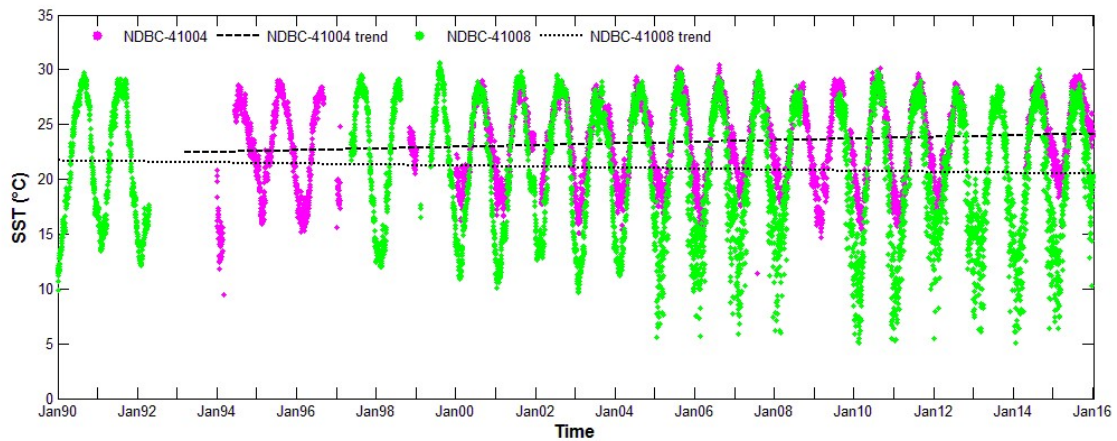

Figure S2. SST trends calculated from moored NDBC time series on the inner (Gray's Reef) and middle (Edisto) shelves.
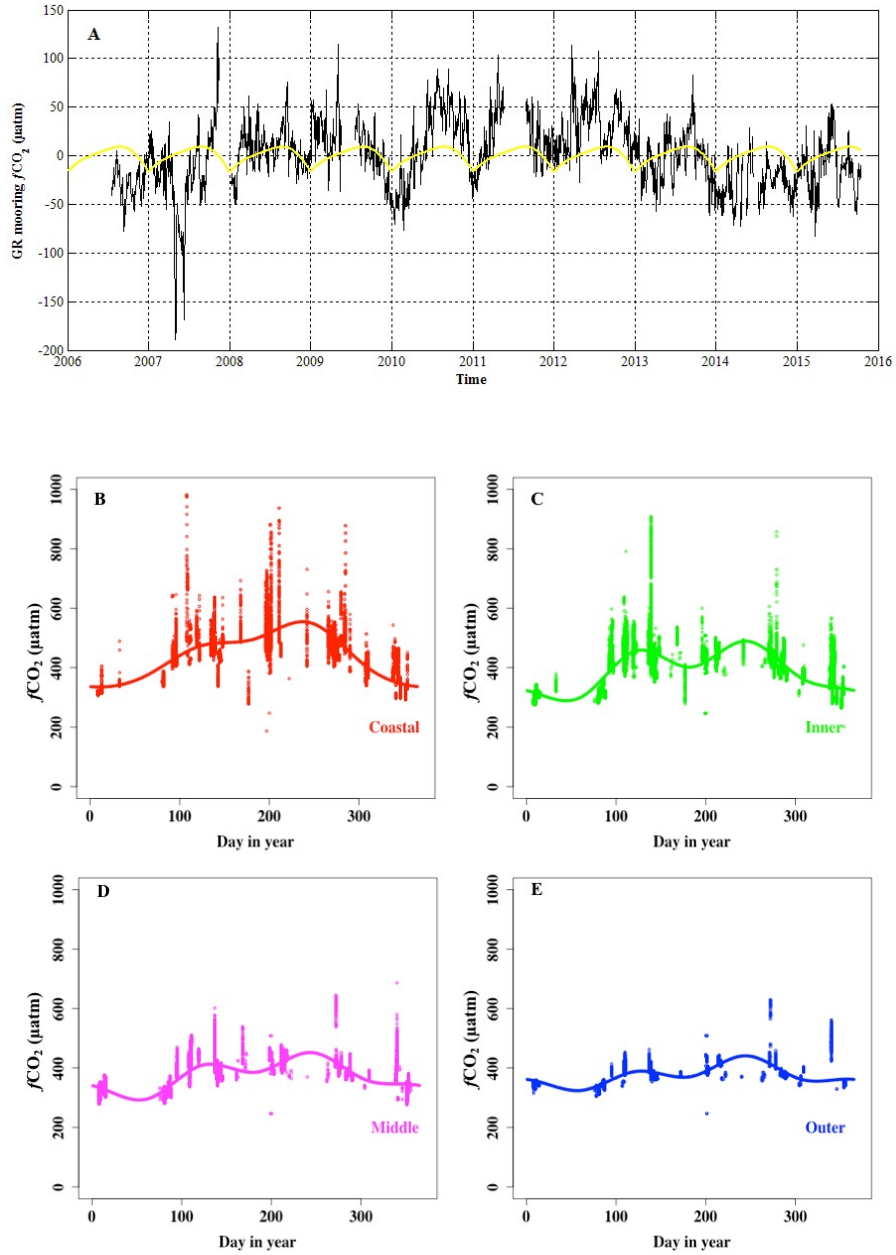
Figure S3. Residual seasonal cycles for (A) the GR mooring $f\mathrm{CO}_2$ time series after deseasonalization using a harmonic method, and region shelf seasonal signals identified through the GAMM: (B) coastal region, (C) inner shelf, (D) middle shelf, and (E) outer shelf. Note that the seasonal signal in panel (A) is superimposed on the anomalies post-deseasonalization.

Table S1. A summary of the cruises used in this work. The date given is the month and year that the cruise was in the SAB. Not all cruises covered all regions. The regions covered are those defined in this work, though are referred to in other publications under their previous definitions. No link to data indicates that these data have not been released to public repositories at the time of publishing.

Date, Ship	SAB regions covered	Link to data[1]	EXPOCODE or Comments
Aug 1991, M/V Le Rabelais[3]	Outer	http://cdiac.ornl.gov/ftp/oceans/ECOA_France/	35RF19910727/ VOO[2]
Oct-Nov1991, M/V Le Rabelais[3]	Outer, middle, inner, coastal	http://cdiac.ornl.gov/ftp/oceans/ECOA_France/	35RF19911022/VOO
Feb 1992, M/V Le Rabelais[3]	Outer, middle, inner	http://cdiac.ornl.gov/ftp/oceans/ECOA_France/	35RF19920216/VOO
June 1992, M/V Le Rabelais[3]	Outer, middle, inner	http://cdiac.ornl.gov/ftp/oceans/ECOA_France/	35RF19920531/VOO
Sept 1992, M/V Le Rabelais[3]	Outer, middle	http://cdiac.ornl.gov/ftp/oceans/ECOA_France/	35RF19920909/VOO
Jan 1994, M/V Le Rabelais[3]	Outer, middle	http://cdiac.ornl.gov/ftp/oceans/ECOA_France/	35RF19931229/VOO
April 1994, M/V Le Rabelais[3]	Outer	http://cdiac.ornl.gov/ftp/oceans/ECOA_France/	35RF19940406/VOO
Aug 1994, M/V Le Rabelais[3]	Outer, middle, inner, coastal	http://cdiac.ornl.gov/ftp/oceans/ECOA_France/	35RF19940731/VOO
May 1995, M/V Le Rabelais[3]	Outer, middle	http://cdiac.ornl.gov/ftp/oceans/ECOA_France/	35RF19950509/VOO
Aug 1995, M/V Le Rabelais[3]	Outer	http://cdiac.ornl.gov/ftp/oceans/ECOA_France/	35RF19950820/VOO
Dec 1995, M/V Le Rabelais[3]	Outer, middle, inner	http://cdiac.ornl.gov/ftp/oceans/ECOA_France/	35RF19951205/VOO
March 1996, M/V Le Rabelais[3]	Outer, middle, inner	http://cdiac.ornl.gov/ftp/oceans/ECOA_France/	35RF19960306/VOO
June 1996, M/V Le Rabelais[3]	Outer, middle, inner	http://cdiac.ornl.gov/ftp/oceans/ECOA_France/	35RF19960606/VOO
Sept 1996, M/V Le Rabelais[3]	Outer, middle, inner	http://cdiac.ornl.gov/ftp/oceans/ECOA_France/	35RF19960911/VOO
Dec 1996, M/V Le Rabelais[3]	Outer, middle	http://cdiac.ornl.gov/ftp/oceans/ECOA_France/	35RF19961210/VOO
Dec 2000,	Middle, inner, coastal		Dedicated SAB cruise
April 2002,	Inner, coastal		Dedicated SAB cruise
June 2002,	Inner, coastal		Dedicated SAB cruise
Oct 2002,	Inner, coastal		Dedicated SAB cruise
Dec 2002,	Inner, coastal		Dedicated SAB cruise
Jan 2005, R/V Cape Hatteras	Outer, middle, inner, coastal	http://www.socat.info/	32KZ20050106/SAB
March 2005, R/V Cape Hatteras	Outer, middle, inner, coastal	http://www.socat.info/	33GC20050315/SAB
July 2005, R/V Cape Hatteras	Outer, middle, inner, coastal	http://www.socat.info/	32KZ20050727/SAB
Oct 2005, R/V Cape Hatteras	Outer, middle, inner, coastal	http://www.socat.info/	32KZ20051008/SAB
Dec 2005, R/V Cape Hatteras	Outer, middle, inner, coastal	http://www.socat.info/	32KZ20051216/SAB
May 2006, R/V Cape Hatteras	Outer, middle, inner, coastal	http://www.socat.info/	32KZ20060517/SAB
June 2007,	Outer, middle, inner, coastal		Dedicated SAB cruise
July 2007, R/V Ronald H. Brown	Outer, middle, inner	http://www.aoml.noaa.gov/ocd/gcc/GOMECC1/data.php	33RO20070711[4]
Aug 2008, R/V Joe Ferguson	Middle, inner, coastal		Dedicated SAB cruise
Dec 2008,	Middle, inner, coastal		Dedicated SAB cruise

May 2009, R/V Joe Ferguson	Middle, inner, coastal		Dedicated SAB cruise
May 2010,	Middle, inner, coastal		Dedicated SAB cruise
April 2011, R/V Savannah	Outer, middle, inner, coastal		Dedicated SAB cruise
Oct 2011, R/V Savannah	Outer, middle, inner, coastal		Dedicated SAB cruise
Feb 2012, R/V Joe Ferguson	Middle, inner, coastal		Dedicated SAB cruise
May 2012, R/V Joe Ferguson	Middle, inner, coastal		Dedicated SAB cruise
Aug 2012, R/V Ronald H. Brown	Outer, middle, inner	http://www.aoml.noaa.gov/ocd/gcc/GOMECC2/	33RO20120721[4]
April 2014, R/V Savannah	Outer, middle, inner, coastal	http://www.socat.info/[5]	33H620140402/SAB
May 2014, R/V Savannah	Outer, middle, inner, coastal	http://www.socat.info/[5]	33H620140515/SAB
July 2014, R/V Savannah	Outer, middle, inner, coastal	http://www.socat.info/[5]	33H620140715/SAB
Nov 2014, R/V Savannah	Outer, middle, inner, coastal	http://www.socat.info/[5]	33H620141103/SAB
Dec 2014, R/V Savannah	Outer, middle, inner, coastal	http://www.socat.info/[5]	33H620141204/SAB
July 2015, R/V Gordon Gunter	Outer, middle, inner, coastal	http://www.aoml.noaa.gov/ocd/ocdweb/gunter/gunter_2015.html	33GG20150708[6]
April 2016, R/V Savannah	Outer, middle, inner, coastal	http://www.socat.info/[5]	33H620160417/SAB

[1]Link to present data repository at the time of acceptance of the manuscript. If no EXPOCODE is given, then the data set has not yet been submitted to a data repository at the time the manuscript was accepted.

[2]Vessel of Opportunity from the Ship of Opportunity Programme

[3]The *M/V Le Rabelais* was formerly named the *M/V Lillooet* in early publications of this data set.

[4]The GOMECC (Gulf of Mexico and East Coast Carbon) cruises extended from the Gulf of Maine to the Gulf of Mexico and each covered a limited area in the SAB.

[5]Data has been submitted to the Surface Ocean Carbon Atlas for quality control as of January 2017 and is scheduled for release .

[6]The ECOA (East Coast Ocean Acidification) cruise extended from the Gulf of Maine to Miami, Florida and covered a greater area of the SAB than the previous GOMECC cruises.